Transient thermal analysis during the ascent phase of a balloon-borne payload. Comparison with SUNRISE test flight measurements

Isabel Pérez-Grande, Angel Sanz-Andrés, Nikolai Bezdenejnykh, Peter Barthol

ABSTRACT

The thermal design of stratospheric balloon payloads usually focuses on the cruise phase of the missions, that is, the floating altitude conditions. The ascent phase usually takes between 2 and 4 h, a very small period compared to the duration of the whole mission, which can last up to 4 weeks. However, during this phase payloads are subjected to very harsh conditions due mainly to the convective cooling that occurs as the balloon passes through the cold atmosphere, with minimum temperatures in the tropo-pause. The aim of this work is to study the thermal behaviour of a payload carried by a long duration balloon during the ascent phase. Its temperature has been calculated as a function of the altitude from sea level to floating conditions. To perform this analysis it has been assumed that the thermal interactions (convection and radiation) depend on the altitude, on the environmental conditions (which in turn depend also on the altitude) and on the temperature of the system itself. The results have been compared with the measurements taken during the SUNRISE test flight, launched in October 2007 by CSBF from Fort Sumner (New Mexico).

1. Introduction

Long Duration Balloon (LDB) scientific experimentation plays a relevant role in the study of the atmosphere (composition, structure and dynamics), and also as a platform for the development of technology for future space missions. Although the environmental conditions are not exactly the same as those found in real space missions, the instruments that carry out the experiments in a LDB can be used as precursors of the instruments to be used in space. These experiments have many advantages over space missions, mainly in terms of costs but also because the payload can be recovered after the flight, which allows a lot of information about the performance of the instrument to be obtained. A review of the use of balloons for scientific purposes can be found in [1].

Depending on the balloon capacity, an LDB can lift up to 3 tons to an altitude of more than 40 km, with missions lasting up to 20 days. The air at this floating altitude is very rarefied, the external pressure is only about 300 Pa, which makes the environment of the payload in terms of heat transfer (dominated by radiation) very similar to the space environment. The main difference with regard to space missions is the presence of uncompensated gravity forces, which obviously act on these types of payloads. For instance, natural convection occurs within pressurized vessels.

Some studies have been made related to the thermal behaviour of LDB balloons [2–5], but they are focussed mainly on the balloon itself rather than on the payload. Little information can be found about the thermal design of balloon payloads and their behaviour during the ascent phase [6,7].

A number of LDBs are launched to circumnavigate the Poles during the summer. These launch sites have many advantages with respect to other geographic locations. First, permanent light in summer, which allows for instance sun observation. Second, in this season winds at floating altitudes are very predictable and therefore the trajectory can be foreseen. Third, the concern about flying over a populated area is notably reduced. The main drawbacks of these sites are, from the design point of view, the extreme environmental conditions and, from the operational point of view, the difficulty to access certain areas to recover the payload after the mission.

The design of payloads requires a thermal analysis as does the whole vehicle. However, prior to these analyses it is necessary to define the design requirements for the flight hardware, namely to establish both the operational and the non-operational temperature limits as well as the temperature gradients and stability. To assess the feasibility of the mission it is necessary to estimate the potential temperature extremes in the worst case scenarios, which have to be previously identified.

Qualitatively, the ascent phase can be a problem, mainly in the Poles where environmental conditions are very harsh. At low altitudes, where the air is still not very rarefied, forced convection and

radiation to space cool the payload. During this phase it is assumed that most devices are switched off, that is, little electrical power is being dissipated as heat. Unfortunately, these cooling effects added to the fact that the air temperature at the tropopause can reach up to −70 °C, can lead to very low temperatures of the systems onboard. The aim of this transient thermal study is to estimate the temperatures that can be reached in the hardware during the ascent period as well as to find the influence of different parameters on this temperature.

2. Sunrise

SUNRISE is a solar observatory based on a telescope with 1 m of diameter that will fly from Esrange within the Long Duration Balloon (LDB) program of NASA. At an altitude of 40 km in the polar summer, constant Sun observation is possible as no night periods occur, with practically the same conditions of observation as from outer space. The aperture of the telescope allows reaching spatial resolutions (diffraction limited) never obtained before from ground during time intervals of hours to days. The high-priority scientific objective of the SUNRISE project is to resolve magnetic structures with spatial scales of the order of 100 km in the solar surface. A CAD view of SUNRISE can be seen in Fig. 1.

SUNRISE is an international collaboration led by the Max Planck für Sonnensystemforschung (MPS, Lindau, Germany) that includes the participation of other institutes such us KIS (Friburgo, Germany), HAO-NCAR (Boulder, USA), IAC (Tenerife, Spain), IAA (Granada, Spain), INTA (Madrid, Spain), IDR-UPM (Madrid, Spain), GACE (Valencia, Spain) and LMSAL (California, USA).

In order to test the pointing system and the capabilities and performance of the hardware, the electronics and software systems of SUNRISE, a test flight was conducted on October, 3rd, 2007. The balloon was launched by the CSBF team from Fort Sumner (New Mexico, USA) at 14:56:44 UT (corresponding to 08:56 h local time, MDT). A float altitude of about 121,000 ft was reached 2:20 h later. The flight was terminated at 23:45 UT (corresponding to 17:45 MDT) after nearly 6.5 h afloat.

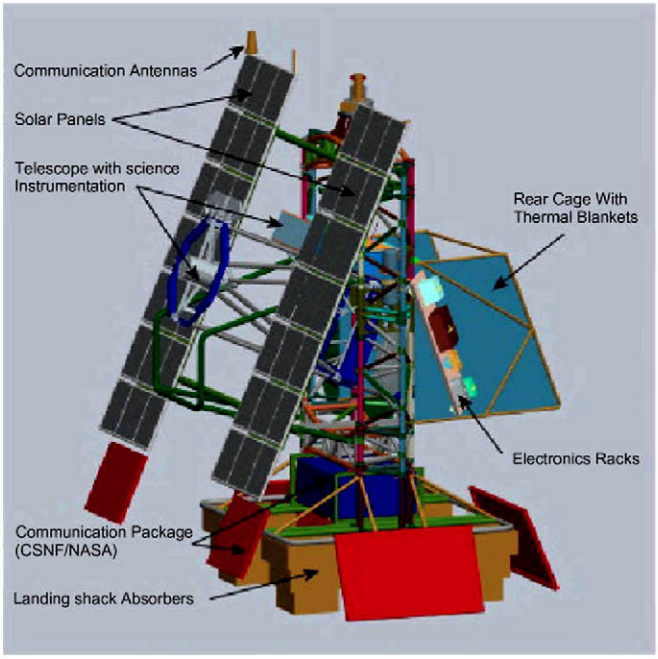

Fig. 1. CAD model of SUNRISE, with the main elements indicated on it.

Part of the science flight equipment was replaced with dummies with the same mass properties as those of the science flight. A picture of the test flight model of SUNRISE is shown in Fig. 2.

3. Problem description

The work presented in this paper consists of two parts: first, the formulation and results for a generic payload, and second, the comparison of the numerical results with the SUNRISE test flight data.

Payloads carried by balloons are usually installed on a mounting structure, that here is called gondola. The devices that are most going to suffer the effects of the outer conditions are those located on the surface of the gondola, as they are the most exposed to both external air and radiation to outer space. This is why the configuration analysed consists of a box attached to the side of the gondola as is shown in Fig. 3. This box represents a generic electronics box with internal dissipation. The area of the front face of the box is A. During the ascent phase of the balloon, the gondola rotates around its vertical axis.

In a first step, the box has been modelled by one single node. When the results are compared with the test flight data, a second node has been included in the model.

4. Governing equation

In order to estimate the temperature of the box during the ascent period, the energy equation for the box has been written as:

$$mc\frac{dT}{dt} = \dot{Q}_{net} + P_{dis} \tag{1}$$

where m is the mass of the box, c is its specific heat capacity, T is its temperature, t is the time, P_{dis} is the power dissipated and $\dot{Q}_{net}$ is

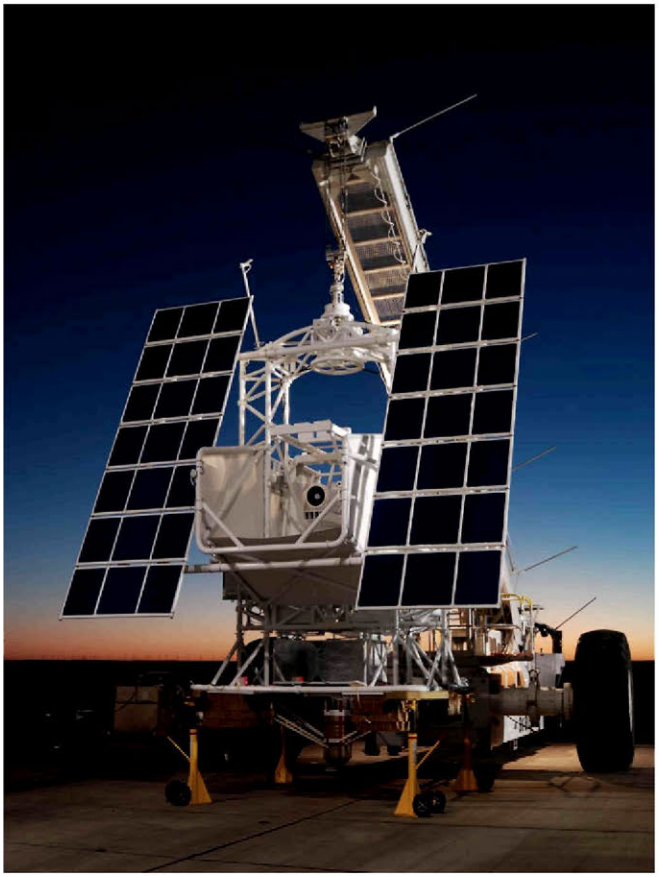

Fig. 2. SUNRISE test flight model.

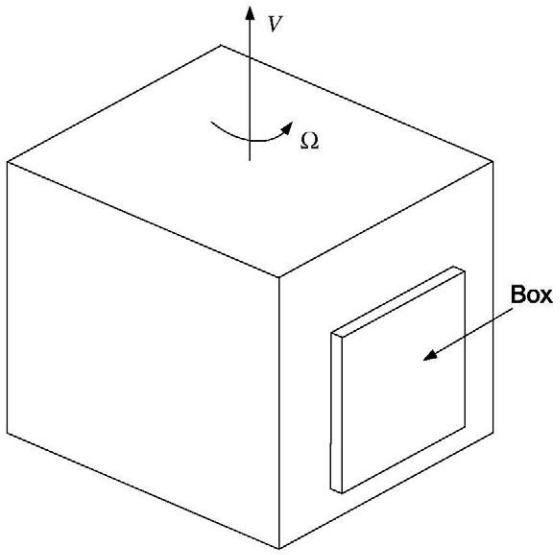

Fig. 3. Sketch of the gondola and the box analysed on it.

the net heat transfer onto the box, which depends on the temperature of the box T, on the environmental conditions and on the altitude H.

The thermal loads onto the box, the radiation and convection, depend on the temperature of the surface, on the temperature of the air and on the altitude. To solve the equation all these thermal loads have been calculated as a function of the altitude. The relation between the altitude H and the time t is obtained assuming that the ascent velocity of the gondola v is constant and therefore: $H = vt$. This hypothesis has been checked with the results of the test flight: the balloon climb up to 15 km with practically constant velocity, and from that point continued up to floating altitude also with constant velocity but slightly higher than during the first phase.

4.1. Thermal interactions

The term $\dot{Q}_{\text{net}}$ is the sum of the radiative, convective and conductive terms: $\dot{Q}_{\text{net}} = \dot{Q}_{\text{rad}} + \dot{Q}_{\text{conv}} + \dot{Q}_{\text{cond}}$. The gondola structure has been considered as a boundary condition for the problem, with a determined temperature that is function of the altitude. The thermal interactions have been estimated as follows:

4.1.1. Radiation interactions

The radiation interactions can be divided into two types: the outgoing radiation emitted by the surface $\dot{Q}_{\text{emitted}}$ and the radiation absorbed by the surface $\dot{Q}_{\text{absorbed}}$. The total radiation to be included in the right hand of Eq. (1) is $\dot{Q}_{\text{rad}} = \dot{Q}_{\text{absorbed}} - \dot{Q}_{\text{emitted}}$.

The outgoing radiation emitted by the surface can be written as $\dot{Q}_{\text{emitted}} = A\varepsilon\sigma T^4$, where ε is the emissivity of the surface and $\sigma = 5.68 \times 10^{-8}\ \text{W m}^{-2}\ \text{K}^{-4}$ is the Stefan–Boltzmann constant.

The absorbed radiation has two components: infrared absorbed radiation and solar (both direct and albedo) absorbed radiation. For the absorbed infrared radiation it is supposed that the box can "see" the Earth, the balloon skin and the sky:

$$\dot{Q}_{\text{infrared absorbed}} = A\varepsilon F_{\text{B-E}}(H)\sigma T_{\text{E}}^4 + A\varepsilon F_{\text{B-bal}}\varepsilon_{\text{bal}}(H)\sigma T_{\text{bal}}^4(H) + A(1 - F_{\text{B-E}}(H) - F_{\text{B-bal}}(H))\varepsilon\sigma T_{\text{sky}}^4(H) \quad (2)$$

where $F_{\text{B-E}}$ is the view factor of the box with respect to the Earth and $F_{\text{B-bal}}$ is the view factor of the box with respect to the balloon, where both depend on the altitude H. They can be calculated from [8], this being the view factor between a sphere and a flat plate:

$$F_{\text{plate-sphere}} = \frac{1}{\pi}\left[\tan^{-1}\frac{1}{\sqrt{S^2-1}} - \frac{\sqrt{S^2-1}}{S^2}\right] \quad (3)$$

where $S = (R_{\text{sphere}} + D)/R_{\text{spehere}}$, R_{sphere} is the sphere radius and D the distance from the sphere surface to the plate. A linear variation with the altitude of the balloon diameter has been used for calculations. At float altitude, a diameter of 130 m has been assumed.

The equivalent black-body temperature for Earth surface T_{E} has been chosen as $T_{\text{E}} = 260$ K, that is, the Earth is radiating 259 W m^{-2}. Regarding the equivalent black-body temperature for the sky T_{sky}, according to [9], the extreme minimum temperature at sea level has been chosen as $T_{\text{sky sea level}} = -30$ °F (≈ -34 °C), that is 239 K. At an altitude of 50 km, the atmosphere is so rarefied that the temperature of the sky is assumed to be equal to the temperature of outer space, $T_{50\text{ km}} = 3$ K. An exponential variation from sea level to that altitude (50 km) for the sky equivalent temperature has been considered, that is,

$$T_{\text{sky}}(H) = T_{\text{sky sea level}} \exp\left(C\frac{H}{50\text{ km}}\right), \quad \text{where } C = \ln\left(\frac{T_{\text{sky 50 km}}}{T_{\text{sky sea level}}}\right)$$

The mean temperature for the balloon skin has been taken from [5].

Concerning the absorbed solar radiation $\dot{Q}_{\text{solar absorbed}}$, there are two contributions to this term: the solar radiation absorbed directly by the box surface and the albedo radiation, which is the diffuse solar radiation reflected on the Earth's surface that is eventually absorbed by the box surface. To obtain these thermal loads four cases have been studied: first, no solar radiation or night case (case 1); second, no direct solar radiation but albedo, that is, the box is facing just opposite the sun direction so that it is shadowed by the gondola (case 2); third, the gondola is rotating with constant angular velocity ω (case 3); and fourth, there is permanent solar irradiation on the box (case 4). The last case would correspond to a limit value of the angular velocity $\omega = 0$, a static position of the box facing the Sun.

The intensity of the solar irradiation G_{s} depends on the altitude due to the absorption and reflection of the atmosphere. According to [9], the dependence of the solar irradiation on the altitude can be calculated from the local atmospheric density. The solar irradiation at sea level $G_{\text{s sea level}}$ and in the outer space $G_{\text{s out}}$ must also be known. The solar irradiation at an altitude H is:

$$G_{\text{s}}(H) = G_{\text{s sea level}} + (G_{\text{s out}} - G_{\text{s sea level}})\left(1 - \frac{\rho(H)}{\rho_{\text{sea level}}}\right)$$

where the air density at an altitude H, $\rho(H)$, will be calculated in the following sections either with the provisions of the International Standard Atmosphere [11] or with experimental data.

When the gondola is rotating with an angular velocity ω, the direct solar irradiation absorbed by the box surface also depends on the angle that the normal vector to the box forms with the sun direction. Let $\beta(t) = \omega t$ be the angle rotated by the gondola. If the sun elevation angle is θ_{s}, then the solar direct absorbed radiation and the albedo absorbed radiation are in each of the cases described above:

- Case 1: no solar radiation (night)

$$\dot{Q}_{\text{direct solar absorbed}} = 0$$
$$\dot{Q}_{\text{albedo solar absorbed}} = 0$$

- Case 2: no direct solar radiation but albedo (shade)

$$\dot{Q}_{\text{direct solar absorbed}} = 0$$
$$\dot{Q}_{\text{albedo solar absorbed}} = \alpha a A F_{\text{B-E}}(H) G_{\text{s}}(H)\sin(0.9\theta_{\text{s}})^{3/2}$$

- Case 3: gondola rotating

$$\dot{Q}_{\text{direct solar absorbed}} = \alpha A G_s(H)\cos(\beta(t))\cos(\theta_s)$$
for $(0 \leqslant \cos(\beta(t)) \leqslant 1)$

$$\dot{Q}_{\text{direct solar absorbed}} = 0 \text{ for } (-1 \leqslant \cos(\beta(t)) \leqslant 0)$$

$$\dot{Q}_{\text{albedo solar absorbed}} = \alpha a A F_{B-E}(H) G_s(H)\sin(0.9\theta_s)^{3/2}$$

- Case 4: permanent solar irradiation

$$\dot{Q}_{\text{direct solar absorbed}} = \alpha A G_s(H)\cos(\theta_s)$$

$$\dot{Q}_{\text{albedo solar absorbed}} = \alpha a A F_{B-E}(H) G_s(H)\sin(0.9\theta_s)^{3/2}$$

where α is the absorptivity of the surface and a is the albedo coefficient. The albedo dependence on the sun elevation angle has been taken for low altitudes from [10].

4.1.2. Convective interactions

The convective interactions are calculated by means of Newton's law of cooling that states:

$$\dot{Q}_{\text{conv}} = -Ah(T - T_{\text{amb}}(H))$$

where h is the heat transfer coefficient and depends on both air and surface temperatures, on the size of the surface and on the velocity of the air passing next to the box. The effect of the rotation of the gondola on the heat transfer coefficient has been neglected.

The coefficient h is calculated through the Nusselt number: $h = k(T_{\text{mean}})Nu/L$, where L is the length of the plate in the direction of the flow, here chosen as $L = A^{1/2}$, and $k(T_{\text{mean}})$ is the thermal conductivity of the air evaluated at a mean temperature between the surface temperature and the free stream temperature: $T_{\text{mean}} = (T + T_{\text{amb}}(H))/2$. The thermal conductivity of air as a function of the temperature is [11]:

$$k(T) = \frac{2.68151 \times 10^{-3} \times T^{3/2}}{T + 245.4 \times 10^{-12/T}} \; W\,m^{-1}\,K^{-1}$$

The Nusselt number depends on whether the flow is laminar or turbulent. The correlations used to calculate this number, according to [12], are written as a function of the Reynolds number and the Prandtl number:

$$Nu = 0.664 Re^{0.5} Pr^{1/3} \quad \text{for } Re \leqslant 5 \times 10^5$$

$$Nu = (0.037 Re^{4/5} - 871) Pr^{1/3} \quad \text{for } 5 \times 10^5 \leqslant Re \leqslant 10^7$$

The Reynolds number Re is defined as:

$$Re = \frac{\rho(H) v L}{\mu(T_{\text{mean}})}$$

where v is the velocity of the air and $\mu(T_{\text{mean}})$ is the viscosity of the air evaluated at the mean temperature between the surface and the free stream air. According to [11] its value is:

$$\mu(T) = \frac{1.458 \times 10^{-6} \times T^{3/2}}{T + 110.4} \; \text{kg}\,m^{-1}\,s^{-1}$$

The Prandtl number is also a function of the temperature: $Pr(T) = 0.804 - 3.25 \times 10^{-4} T$.

Once the Reynolds number has been calculated, the Nusselt number and subsequently the heat transfer coefficient can be evaluated to obtain the convective interactions as a function of the temperature and of the air temperature.

4.1.3. Conductive interactions

In the initial analysis, the box has been considered thermally insulated from the gondola. When comparing with experimental data the conductive interactions are calculated by means of the equation:

$$\dot{Q}_{\text{cond}} = -C(T - T_{\text{gondola}}(H))$$

The gondola temperature and the thermal coupling coefficient C have been calculated from experimental data.

4.2. Atmospheric model

To calculate all the interactions described in the previous subsections it is necessary to define a model for the environmental conditions. The International Standard Atmosphere ISA described in [11] and ISA–15 described in [13] have been used for the general study. When comparing with test flight data, experimental data for the atmosphere have been used.

5. Results

Once the thermal loads and the properties of the atmosphere are defined, taking into account the relation between the altitude and the time, Eq. (1) can be rewritten as

$$mc\frac{dT}{dt} = f(T, t)$$

where the right hand is a function of both temperature and time.

The equation is solved to obtain $T(t)$ using a Runge-Kutta (fourth order) method. The input data taken as reference values throughout all the calculations are: ascent speed $v = 10$ km/h, air temperature at sea level $T_{\text{amb}}(0) = 20\,^{\circ}\text{C}$, initial temperature at sea level $T(0) = 20\,^{\circ}\text{C}$, area of the box surface $A = 0.2\ \text{m}^2$, mass of the box $m = 2.0$ kg, specific heat capacity $c = 900\ \text{J kg}^{-1}\,\text{K}^{-1}$, solar irradiation at sea level $G_{s\ \text{sea level}} = 700\ \text{W m}^{-2}$, rotation speed $\omega = 1$ rpm, Sun elevation angle $\theta_s = 25\,^{\circ}$, solar absorptivity $\alpha = 0.2$, emissivity $\varepsilon = 0.8$ (corresponding to a white paint), albedo coefficient $a = 0.3$, and dissipated power $P_{\text{dis}} = 20$ W. These values correspond to the baseline configuration. Fig. 4 shows the radiation and convection heat losses, the albedo, the solar radiation and the Earth infrared radiation absorbed by the box. The convective cooling has a maximum effect close to the tropopause. From that point its value decreases to be virtually negligible at floating altitude. The changes of slope observed in the convection heat losses correspond to the changes of slope in the air temperature profile.

In the following, the sensitivity analysis of influence of these parameters is performed.

The results have been plotted with the altitude H in the ordinates axis, as it is usually done when studying atmospheric profiles.

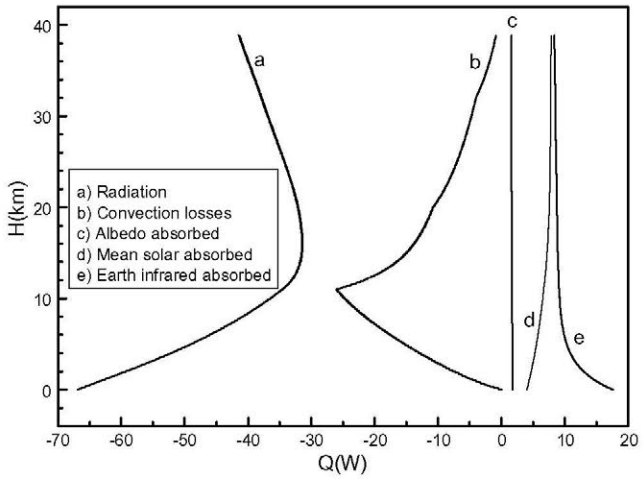

Fig. 4. Radiation and convection heat losses and mean solar radiation, albedo and Earth infrared radiation absorbed by the box versus altitude, H.

5.1. Influence of thermal inertial properties

The product *mc*, the heat capacity, is a measurement of the thermal inertia of the system. The higher the value of *m c* the lower the influence of the external loads on the temperature of the box. Fig. 5 shows the influence of this parameter. The results have been obtained for $mc = 1800$, 3600 and 5400 J K^{-1}. The profiles are slightly wavy due to the rotation of the gondola that originates oscillating thermal loads and therefore oscillating temperature values.

5.2. Influence of the rotation velocity of the gondola

Fig. 6 shows the influence of the rotation velocity of the gondola on the temperature of the box. The results have been obtained for $\omega = 0.1$ and 1 rpm. When $\omega = 0.1$ rpm, very slow rotation, the wavy effect of the rotation on the temperature is notably increased: in this case the temperature of the box oscillates with a higher amplitude.

5.3. Influence of solar radiation

Fig. 7 shows the temperature profiles in the four cases described in Section 4.1.1: night, no direct solar radiation but albedo, gondola rotating with $\omega = 1$ r.p.m. and permanent solar irradiation. Obviously, the temperature increases as the exposure to solar radiation increases. In this figure it can be seen that the chilling effect of cold air affects mainly up to an altitude of about 11 km. From this point, temperature starts to rise.

5.4. Influence of the ascent velocity

Fig. 8 shows the temperature profiles for three values of ascent velocity: $v = 5$, 10 and 15 km/h. Two opposite effects are found here: on the one hand, the higher the value of the ascent speed the higher the cooling effect of the air and therefore, for a determined altitude, lower temperatures should be encountered. However, on the other hand, if the ascent speed is slower the system is closer to finding thermal equilibrium with the air. Note that in this figure the altitude scale does not correspond with the time scale.

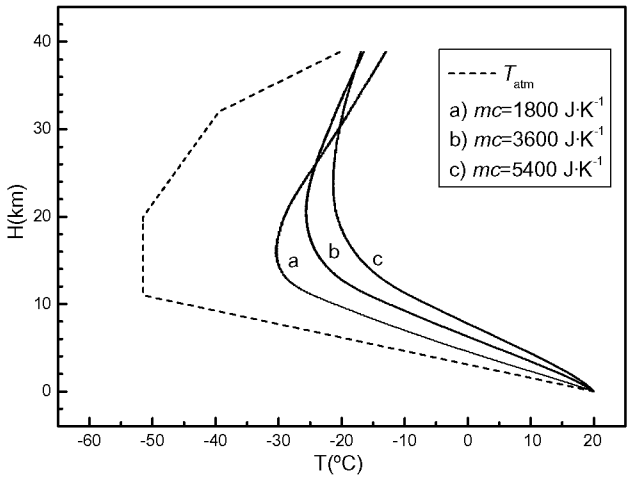

Fig. 5. Temperature, *T*, versus altitude, *H*, of both the atmospheric air (dashed line) and the box (solid lines) for different values of the thermal inertia *mc*.

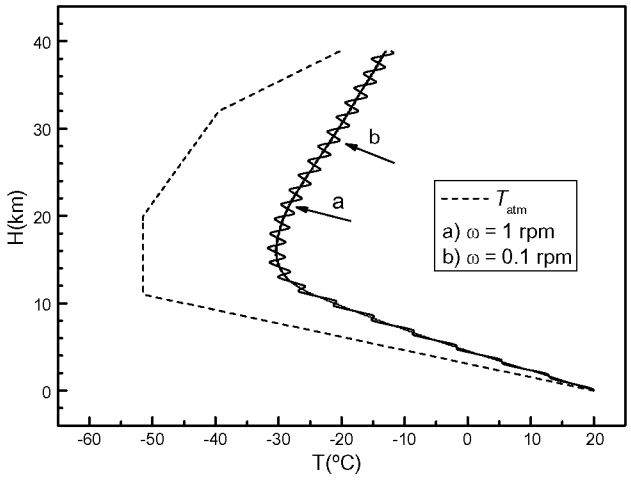

Fig. 6. Temperature, *T*, versus altitude, *H*, of both the atmospheric air (dashed line) and the box (solid lines), plotted for for $\omega = 0.1$ and 1 rpm.

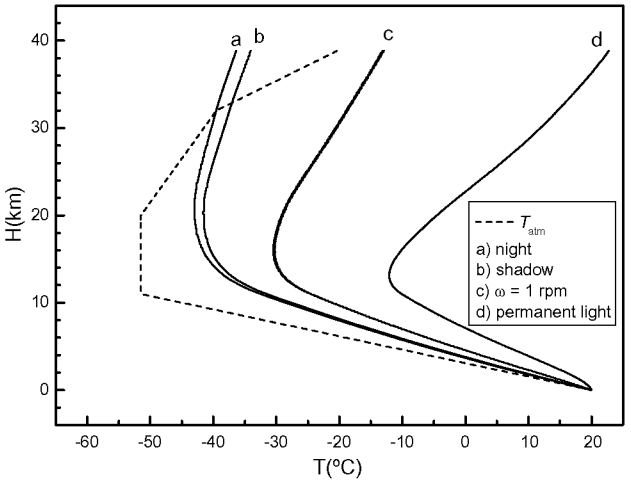

Fig. 7. Temperature, *T*, versus altitude, *H*, of both the atmospheric air (dashed line) and the box (solid lines). The box temperature profile has been plotted for night conditions (*a*), no direct solar radiation but albedo (*b*), $\omega = 1$ rpm (*c*) and permanent solar irradiation (*d*).

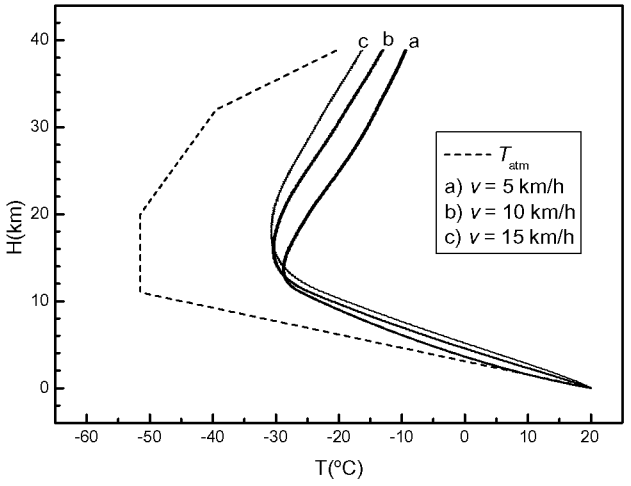

Fig. 8. Temperature, *T*, versus altitude, *H*, of both the atmospheric air (dashed line) and the box (solid lines). The box temperature profile has been plotted for different values of the ascent speed as indicated in the figure.

6. Comparison with SUNRISE test flight data

Once a general model has been set up to study the thermal behaviour during the ascent phase of a generic payload, the model has been applied to one of the electronics boxes carried during the SUNRISE test flight: ICU. This box was instrumented with thermocouples to monitor its temperature.

In order to compare the theoretical analysis with the flight measurements, the Standard Atmosphere model has been replaced by functions that fit the atmospheric data. So, the atmospheric temperature profile consists of two linear sections; each one fits the data corresponding to each of the two constant temperature rate changes that the ascent phase consists of. The atmospheric temperature profile is shown in Figs. 9 and 10, with the model results. In this case, for better comparison, the temperature has been plotted in the ordinates axis.

Since, after the test flight, there are quite a lot of ICU data available to study its thermal behaviour, two different approaches have been considered for this box: first the whole box has been considered as a single node, and second an additional inner node has been included in the model to study the difference of performance of the housing and the electronics itself.

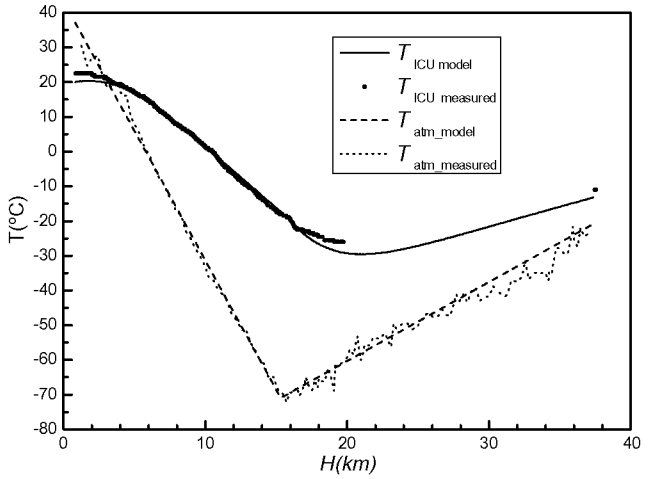

Fig. 9. Temperature, T, versus altitude, H, of the atmospheric air (measured and linear approach) and of the box (measured and model results).

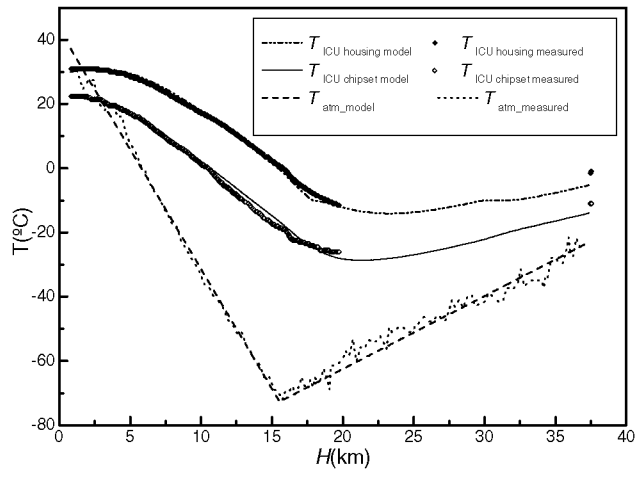

Fig. 10. Temperature, T, versus altitude, H, of the atmospheric air (measured and linear approach) and of the box housing and inner chipset (measured and model results).

6.1. Single node ICU model

Eq. 1 has been directly applied to ICU. The parameters in the equation have been adjusted to ICU's: $A = 0.19\ m^2$, $m = 4.5$ kg, $P_{dis} = 35$ W. Two constant ascent speed periods with $v = 19$ km/h up to an altitude of 15.7 km and $v = 15$ km/h from 15.7 km have been considered. The other parameters remain the same as in the previous sections. Fig. 9 shows the results of the analytical model for ICU (continuous line) as well as the measured data (scattered points). During the second part of the ascent data transmission was interrupted due to the malfunction of one of the electronics devices, presumably because of subcooling beyond the lower temperature limits. Nevertheless, there are enough data available to validate the theoretical model. As can be seen in the figure, the theoretical model results and the measured data are in good agreement, mainly during the first part of the ascent. Differences less than 5 °C are found during the second part of the ascent period most likely because of the fluctuating atmospheric conditions.

6.2. Two-node ICU model

In this case a set of two ordinary differential equations has been written and solved in order to study the behaviour of the housing and the electronics components. Eq. 1 has been written twice, firstly to be applied to the inner node where dissipation is applied, and secondly to be applied to the outer node, which is subjected to the environmental thermal interactions. The thermal coupling between the inner and the outer node has been adjusted to match the experimental results. The temperature of the 'chipset' has been monitored during the test flight and is used here as reference of the inner node. Fig. 10 shows the temperatures of the ICU housing and chipset obtained with the model as well as the data. As in the previous section the model and the flight data are in good agreement mostly during the first part of the ascent.

7. Conclusions

The transient thermal behaviour of a balloon borne payload has been studied. The aim was to set up a model as realistic as possible but also as simple as possible. To achieve this, the main thermal interactions (solar radiation, albedo, Earth infrared radiation, balloon radiation exchange, radiation to outer space and convection) have been taken into account. The relative importance of each term has been presented.

As expected, it has been shown that temperature decreases with the altitude, reaching its minimum value close to the tropopause. The cooling effect of forced convection during the ascent leads to quite low temperatures of the payload, a fact that has to be taken into account in the design phase, i.e. although the design is usually focused on the cruise phase, the ascent phase also has to be carefully analysed, as a cold case for the thermal control subsystem design.

The predictions of the model have been compared with flight data, showing quite good agreement.

Measured values of atmospheric properties are quite lower than those provided by International Standard Atmosphere models, so that working with local atmospheric models is recommended.

Acknowledgements

This work has been supported by the Spanish Ministerio de Educación y Ciencia, Project ESP2006-13030-C06-05 and the German Bundesministerium für Wirtschaft und Technologie through Deutsches Zentrum für Luft und Raumfahrt e.V. (DLR), Grant No. 50 OU 0401.

References

[1] J. Blamont, History and perspectives of scientific ballooning, ESA SP-471, 2001.
[2] H.M. Cathey Jr., Scientific balloon effective radiative properties, Advances in Space Research 21 (1998) 979–982.
[3] H. Franco, H.M. Cathey Jr., Thermal performance modeling of NASA's scientific balloons, Advances in Space Research 33 (2004) 1717–1721.
[4] H.M. Cathey, Transient thermal loading of natural shaped balloons, AIAA, A97-31338, 1997.
[5] R.E. Farley, Balloon Ascent: 3-D simulation tool for the ascent and float of high altitude balloons, A IAA 2005-7412, 2005.
[6] D. Clark, S. Spencer, Thermal design of high altitude balloon gondolas for the Antarctic, AIAA 94-0302, 1994.
[7] S. Spencer, D. Clark, T.A. Parnell, The design and analysis of the thermal control system for the JACEE high altitude long duration balloon flight, Advances in Space Research 17-9 (1996) 91–94.
[8] J.R. Howell, Catalog of Radiation Configuration Factors, McGraw-Hill, 1982.
[9] NASA Technical Memorandum 4511, Terrestrial environment (climatic) criteria guidelines for use in aerospace vehicle development, 1993 revision.
[10] Techniques et Technologies des Vehicules Spatiaux V. 3 Plates-formes, CNES, 1998.
[11] Properties of a standard atmosphere ESDU 77021, The Royal Aeronautical Society, Release 2004-02.
[12] Y.A. Cengel, Heat Transfer: A Practical Approach 1998, McGraw-Hill.
[13] Physical properties of design atmospheres, ESDU 78008, The Royal Aeronautical Society, Release 2004-02.